Fast-ion redistribution and loss due to edge perturbations in the ASDEX Upgrade, DIII-D and KSTAR tokamaks

2013 Nucl. Fusion 53 123008

(http://iopscience.iop.org/0029-5515/53/12/123008)

Nucl. Fusion **53** (2013) 123008 (9pp) doi:10.1088/0029-5515/53/12/123008

Fast-ion redistribution and loss due to edge perturbations in the ASDEX Upgrade, DIII-D and KSTAR tokamaks

M. Garcia-Munoz[1], S. Äkäslompolo[2], O. Asunta[2], J. Boom[3], X. Chen[4], I.G.J. Classen[3], R. Dux[5], T.E. Evans[6], S. Fietz[5], R.K. Fisher[6], C. Fuchs[5], B. Geiger[5], M. Hoelzl[5], V. Igochine[5], Y.M. Jeon[7], J. Kim[7], J.Y. Kim[8], B. Kurzan[5], N. Lazanyi[9], T. Lunt[5], R.M. McDermott[5], M. Nocente[10,11], D.C. Pace[6], T.L. Rhodes[12], M. Rodriguez-Ramos[1], K. Shinohara[13], W. Suttrop[5], M.A. Van Zeeland[6], E. Viezzer[5], M. Willensdorfer[14], E. Wolfrum[5] and the ASDEX Upgrade, DIII-D and KSTAR Teams

[1] FAMN Department, Faculty of Physics, University of Seville, 41012 Seville, Spain
[2] School of Science, Aalto University, PO Box 14100, FI-00076 AALTO, Finland
[3] FOM Institute DIFFER*-Association EURATOM-FOM, 3430 BE, The Netherlands
[4] School of Physical Sciences, University of California-Irvine, Irvine, CA 92697, USA
[5] Max-Planck-Institut für Plasmaphysik, EURATOM Association, D-85748, Germany
[6] General Atomics, San Diego, CA, 92186-5608, USA
[7] National Fusion Research Institute, Daejeon 305-806, Korea
[8] Department of Nuclear Fusion and Plasma Science, University of Science and Technology, Daejeon 305-330, South Korea
[9] BME NTI, Association EURATOM, Pf 91, H-1521 Budapest, Hungary
[10] Dipartimento di Fisica 'G. Occhialini', Università degli Studi di Milano-Bicocca, Piazza della Scienza 3, 20126, Milano, Italy
[11] Istituto di Fisica del Plasma Piero Caldirola EURATOM- ENEA-CNR, 20125, Milan, Italy
[12] Department of Physics and Astronomy, University of California-Los Angeles, Los Angeles, CA 90098, USA
[13] JAEA, 801-1, Mukouyáma, Naka City, Ibaraki, 311-0193, Japan
[14] Technische Universität Wien, Association EURATOM-AW, Vienna, Austria

E-mail: Manuel.Garcia-Munoz@ipp.mpg.de

Received 5 May 2013, accepted for publication 10 October 2013
Published 12 November 2013
Online at stacks.iop.org/NF/53/123008

Abstract
The impact of edge localized modes (ELMs) and externally applied resonant and non-resonant magnetic perturbations (MPs) on fast-ion confinement/transport have been investigated in the ASDEX Upgrade (AUG), DIII-D and KSTAR tokamaks. Two phases with respect to the ELM cycle can be clearly distinguished in ELM-induced fast-ion losses. Inter-ELM losses are characterized by a coherent modulation of the plasma density around the separatrix while intra-ELM losses appear as well-defined bursts. In high collisionality plasmas with mitigated ELMs, externally applied MPs have little effect on kinetic profiles, including fast-ions, while a strong impact on kinetic profiles is observed in low-collisionality, low q_{95} plasmas with resonant and non-resonant MPs. In low-collisionality H-mode plasmas, the large fast-ion filaments observed during ELMs are replaced by a loss of fast-ions with a broad-band frequency and an amplitude of up to an order of magnitude higher than the neutral beam injection prompt loss signal without MPs. A clear synergy in the overall fast-ion transport is observed between MPs and neoclassical tearing modes. Measured fast-ion losses are typically on banana orbits that explore the entire pedestal/scrape-off layer. The fast-ion response to externally applied MPs presented here may be of general interest for the community to better understand the MP field penetration and overall plasma response.

(Some figures may appear in colour only in the online journal)

1. Introduction

High confinement regimes in tokamak plasmas [1] are characterized by edge transport barriers (ETBs) [2] that develop rather steep edge pressure gradients ∇p which destabilize large-scale edge localized modes (ELMs) [3] causing intermittent relaxation of edge kinetic profiles. Heat loads induced by unmitigated ELMs on plasma facing components will likely be intolerable in ITER [4, 5]. This could actually be the case for unmitigated inter-ELM cross-field transport also [6]. The successful realization of fusion relies, therefore, in a thorough understanding of edge stability and ELM control. In theory, ELMs can be avoided if the averaged ∇p is reduced by widening the steep gradient region [7]. In present fusion devices, this is obtained through externally applied resonant and non-resonant magnetic perturbations (MPs) [8–11]. MPs have demonstrated their potential to mitigate/suppress ELMs as well as to control resistive wall modes (RWMs) [12], neoclassical tearing modes (NTMs) [13] and plasma rotation [14]. However, results obtained in different machines are not clearly aligned, e.g. different conditions for ELM suppression in DIII-D and AUG [10, 11], which emphasizes the importance of taking into account the plasma response when interpreting the effects of 3D externally applied MPs. Indeed, the plasma response is a key ingredient in determining the stability evolution as the plasma can amplify, suppress or modify a perturbation. Extensive theoretical, modelling and computational efforts have led to an enormous progress. However, neither standard fluid simulations based on the baseline plasma transport theory in stochastic magnetic fields [15] nor the most advanced two-fluids, kinetic nor hybrid simulations have successfully explained the full ELM cycle nor the plasma response to externally applied MPs, especially when anomalous transport needs to be considered self-consistently [16, 17]. Kinetic effects become of special importance to assess plasma stability in low-collisionality burning plasmas with a significant suprathermal (fast) ion content [18]. Fast-ions are indeed an essential source of momentum and energy that under certain conditions may drive directly, or contribute to the development of some, MHD fluctuations that may, in turn, have deleterious effects on global plasma confinement parameters. While kinetic effects of the thermal plasma (ions) have been recognized as an important ingredient in the ELM cycle and its mitigation through MPs, little effort has been invested so far in including a kinetic treatment of fast-ions in modelling and computational tools. This is, in part, certainly due to the lack of accurate fast-ion measurements in the area of interest ($\rho_{\rm pol} \geqslant 0.6$) as well as associated losses with ELMs and MPs. In this paper we will present the latest experimental results obtained in AUG, DIII-D and KSTAR on ELM and MP-induced fast-ion dynamics. As a result of a collaborative work on energetic particles, the AUG, DIII-D and KSTAR tokamaks are now equipped with a set of state-of-the-art fluctuations and fast-ion diagnostics such as scintillator based fast-ion loss detectors (FILDs) [19–21] and fast-ion D-alpha (FIDA) spectroscopy systems [22, 23]. Large bandwidth FILD systems have shown the strong impact that ELMs and MPs can have on fast-ion losses in escaping-ion velocity-space revealing, at the same time, important details on inter- and intra-ELM fluctuations. Active FIDA measurements have been used to monitor the temporal evolution of confined fast-ions during ELMs and MP mitigated ELMy phases. Passive FIDA and neutral particle analyser (NPAs) are typically used to complement FILD signals with independent measurements of fast-ion losses. Internal fluctuation measurements are provided by electron cyclotron emission- (ECE) [24], imaging (ECE-I) [25], soft x-ray (SXR) [26] and reflectometry [27] diagnostics.

2. ELM-induced fast-ion losses

ELM-induced fast-ion losses have been studied in the AUG, DIII-D and KSTAR tokamaks at different positions with a set of FILD systems in plasmas with different collisionalities, $\beta_{\rm N}$ and q_{95}. Figure 1 illustrates typical ELM-induced fast-ion losses measured by FILD systems over many ELM periods with a zoom of one ELM cycle. Two phases can be clearly distinguished in ELM-induced fast-ion losses with respect to the ELM cycle (inter- and intra-ELM losses). Both phases have been highlighted in grey and black in figure 1(*b*) and are described in the next two paragraphs.

2.1. Inter-ELM losses

In AUG and DIII-D low-density H-modes, a coherent modulation of the edge density, observed often just before the ELM crash, correlated with a loss of fast-ions (the amplitude of which increases towards the ELM crash). The pre-ELM density fluctuation is measured in AUG with high spatio-temporal resolution by means of the lithium beam diagnostic [28]. Figure 1 gives an overview of such a phase with the measured divertor current as ELM monitor, the edge density fluctuation measured by lithium beam and the fast-ion losses with energies $E \approx 80$ keV and two different pitch angles 60° and 75°. Figure 1(*a*) shows a time window with several ELMs where the increasing losses towards the ELM crashes are clearly visible. A zoom of an ELM cycle, figure 1(*b*), shows a clear phase-correlation between the measured fluctuations in Li-beam and the pre-ELM fast-ion losses. It is worth noting that the amplitude of the measured fast-ion losses grows towards the ELM crash while the amplitude of the density fluctuation remains at a rather constant value. The density fluctuation propagates in the ion diamagnetic drift direction with a toroidal mode number $n = 2$ as determined by means of the magnetic pick-up coils. This low-frequency pre-ELM fluctuation is typically observed in low-collisionality, high-beta plasmas, reassembling some similarities with the energetic particle driven wall mode (EWM) observed at JT-60U [18] although a detailed characterization of the mode as well as of the conditions under which it is driven unstable still need to be carried out to unequivocally identify it.

In DIII-D, Doppler backscattering reflectometry shows a similar correlation between the oscillations in the fast-ion losses and those in the pedestal flows, indicating a possible effect of a non-ambipolar particle flux on the radial electric field (E_r), see figure 2. In order to estimate, however, the electrodynamic consequences of the escaping fast-ion current, a detailed analysis is necessary [29, 30]. The velocity-space of the escaping ions measured with the DIII-D midplane FILD (FILD2) is shown in figure 3(*a*). In general, pre-ELM losses

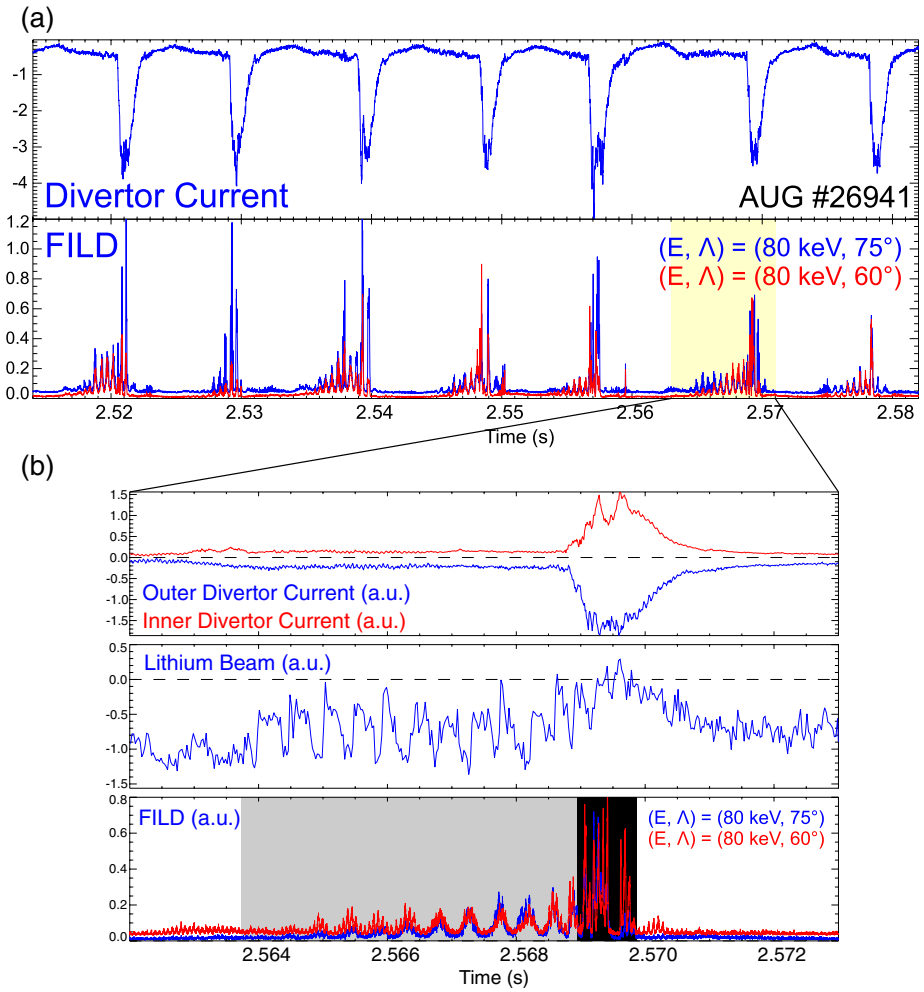

Figure 1. AUG discharge #26941. Fast-ion losses during an ELM cycle and correlation with edge density fluctuations. (*a*) Time traces of fast-ion losses and measured divertor currents at the outer divertor plate. (*b*) Divertor currents at inner (red) and outer (blue) targets, density fluctuations at the separatrix (Li-beam) and FILD signals.

appear typically in a region that corresponds to deuterium ions with energies between 45 keV in DIII-D (with maximal injection energy $E_{\mathrm{NBI}} = 80$ keV) and 80 keV for AUG (with $E_{\mathrm{NBI}} = 93$ keV) and pitch-angles between 70° and 85°. Figures 3(*b*) and (*c*) show a typical measured fast-ion trajectory traced backwards in time from FILD2 to the plasma in a DIII-D EFIT equilibrium. No overlapping between the ion trajectory and the neutral beam injection (NBI) footprint is observed indicating that the observed losses are not NBI prompt losses due to a change in the density of the pedestal/scrape-off-layer (SOL) during the ELM cycle.

2.2. *Intra-ELM losses*

The fast-ion losses associated with the highly non-linear phase of an ELM cycle (crash and post-crash) are studied in 3D with an array of FILD systems located at different toroidal and poloidal positions in AUG and DIII-D. Overall, FILD measures bursting ELM-induced fast-ion losses that are an order of magnitude higher than the nominal NBI prompt loss signal and comparable to most of the MHD-induced fast-ion loss. Surprisingly, in low-collisionality H-modes, intra-ELM fluctuations in fast-ion losses appear connected with basic ELM properties (amplitude and frequency), i.e. high frequency small ELMs are often accompanied by large fluctuating fast-ion losses.

In AUG, well-defined bursts of fast-ion losses are observed with type-I ELMs, suggesting a strong interaction between fast-ions and the fluctuations concomitant to the ELM crash and subsequent blobs/filaments. Two FILD units located ≈30 cm above the midplane and 113° toroidally apart measure most of the bursts simultaneously, indicating the toroidal and poloidal extension of the loss mechanism and particle source. In this regard, as introduced in the previous section, no correlation is found with the density flush in the pedestal/SOL following the ELM crash indicating that the loss mechanism is directly connected to the ELM electromagnetic perturbation rather than to an increase in the NBI prompt losses due to a transient enhancement of the density in the SOL. The most prominent losses are observed in low-collisionality type-I ELMs. This is, in fact, expected from the peeling–ballooning theory where the ELM radial extension depends, among other parameters, on pedestal density/collisionality [7]. Up to 5–6 fast-ion bursts are observed at each type-I ELM with each burst lasting for ≈0.2 ms at full-width half-maximum (FWHM)

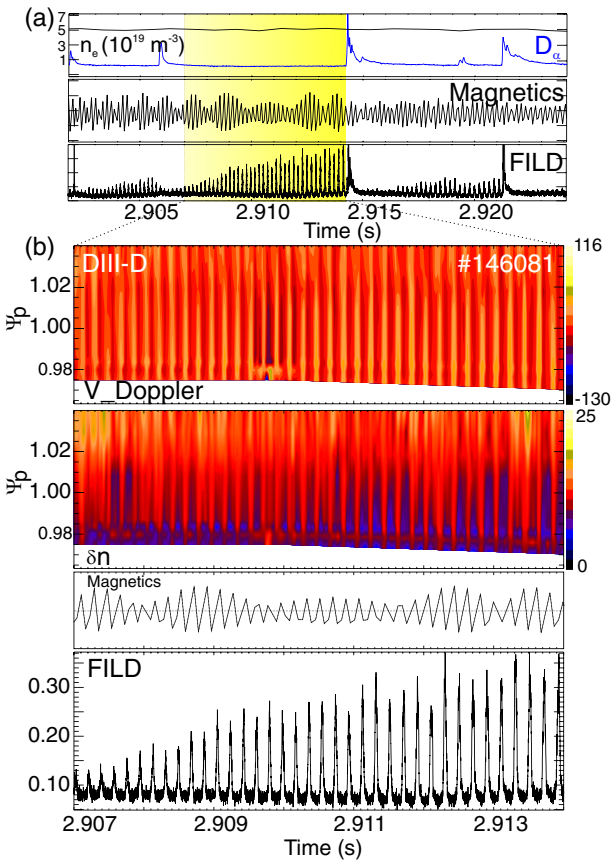

Figure 2. DIII-D discharge #146081. Fast-ion losses during ELM cycle and correlation with edge flow. (*a*) Time traces of density (n_e), ELM monitoring signal (D_α), magnetics and FILD. (*b*) Velocity and density fluctuations measured with backscattering Doppler reflectometry, magnetic fluctuation and fast-ion losses during a pre-ELM crash phase, zoom of (*a*).

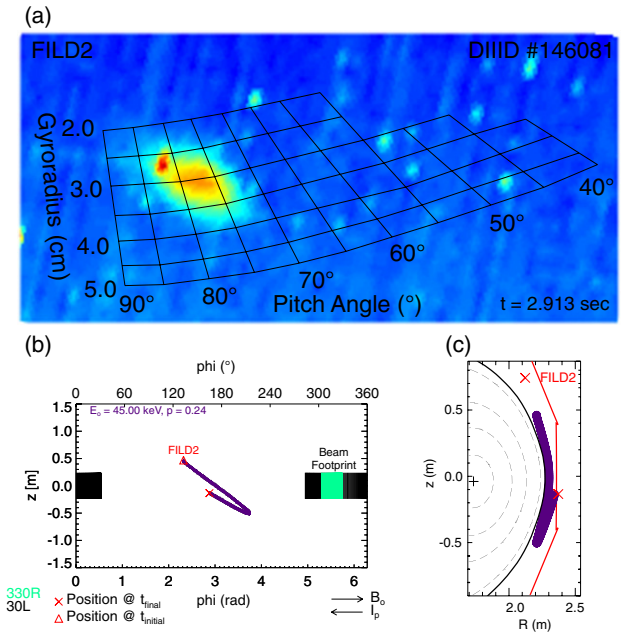

Figure 3. DIII-D discharge #146081. Orbit topology of escaping ions during ELMs measured with FILD2 at DIII-D. (*a*) CCD frame of FILD2 at DIII-D showing the velocity-space of the measured escaping-ions. (*b*) and (*c*) show the projection of the measured fast-ion orbit traced backwards in time in the z–ϕ and z–R plane respectively.

and with ≈0.2 ms between fast-ion bursts. In escaping-ion velocity-space, bursts within a single ELM often show significant changes in the energy and pitch angle of the lost ions while most of the escaping ions are on trapped orbits with energies $E \approx 80$ keV. In DIII-D, however, intra-ELM losses follow more closely the envelope of the D_α signal as it can be seen in figure 2 with most of the lost ions on banana orbits.

3. MP-induced fast-ion dynamics

The fast-ion dynamics induced by MPs have been studied in the AUG and KSTAR tokamaks in H-mode plasmas with a wide range of collisionalities. In AUG, ELM mitigation by 3D externally applied MPs is achieved above a certain density, $\approx 0.6 n_{GW}$ and a rather high collisionality with little to no effect on plasma profiles [11]. In low-collisionality and q_{95} discharges in AUG and KSTAR, however, a strong impact on kinetic profiles is observed, i.e. density pump-out and plasma braking, which is accompanied by a dramatic effect on fast-ion dynamics. We will report here on the effect of MPs on kinetic profiles including fast-ion dynamics in KSTAR and AUG with $n = 1$ and $n = 2$ externally applied MPs, respectively.

3.1. Plasma response to applied MPs

A series of plasma discharges with B_t ranging from -2.5 to -1.8 T, $I_p = 0.8$ MA, $n_e \approx (2\text{–}6) \times 10^{19}$ m^{-3} and a wide set of configurations of the external coils responsible for the MPs have been carried out in the AUG and KSTAR tokamaks. Resonant and non(off)-resonant $n = 1$ and $n = 2$ coil configurations have been used to study the plasma response in low-collisionality discharges. In AUG plasmas with $B_t = -2.5$ T, the current of the coils was set to $I_{coil} \approx 5.0$ kA while for the discharges with $B_t = -1.8$ T, $I_{coil} \approx 5.9$ kA due to the weaker magnetic forces which could make a damage on the hardware, created in the coils with a lower B_t. In KSTAR, the MP coils are powered with up to 8 kA in non-resonant configurations and up to 5 kA in resonant configurations to avoid disruptions due to the strong plasma response to externally applied resonant MPs. The 3D dynamics of the plasma response to the applied MPs have been studied using the AUG comprehensive suite of plasma diagnostics (located at different positions) including Thomson scattering (TS), lithium beam, ECE, DCN, charge-exchange recombination spectroscopy (CXRS) [31], 2D plasma imaging at different wavelengths and MHD spectroscopy. In all discharges a significant density pump-out of up to 30% is clearly observed and is typically accompanied by a marginal ELM mitigation. The electron and ion temperatures, T_e and T_i, are weakly affected and the strongest plasma braking is observed in the presence of a magnetic island with $n_{island} = n_{MP}$. Figure 4 gives an overview of a typical discharge with a resonant $n = 2$ MP configuration. Figure 5 shows the temporal evolution of the kinetic profiles when resonant $n = 2$ MPs are applied in the AUG tokamak. As outlined in the previous section, a clear density pump-out is observed while T_e is not affected

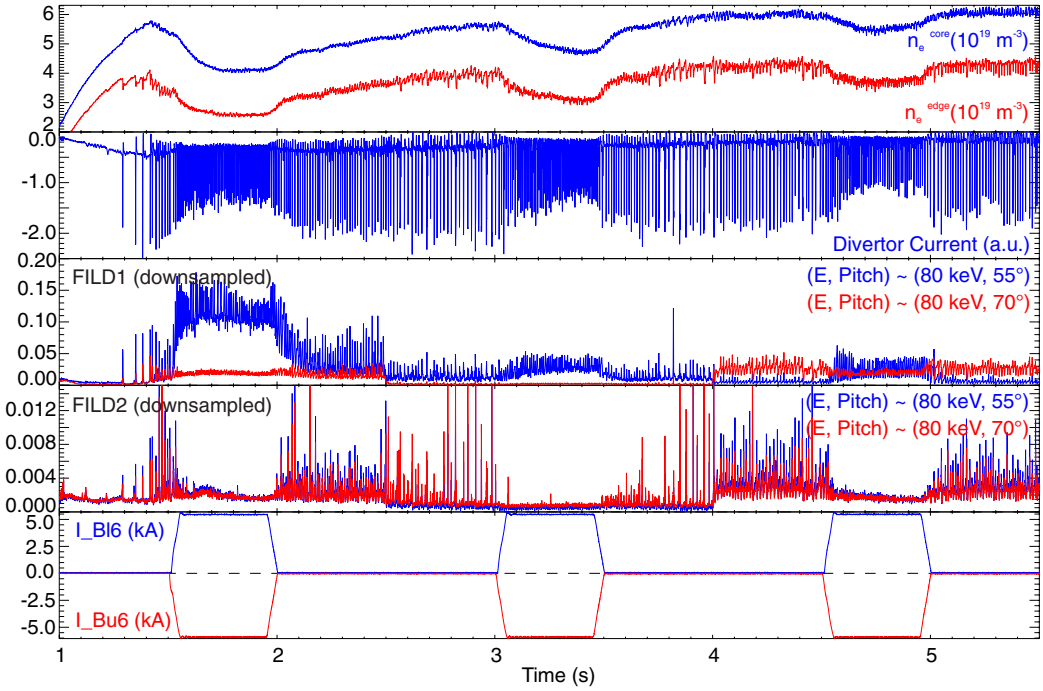

Figure 4. AUG discharge #28061. Overview of discharge with line-integrated core and edge electron density, divertor current at outer target, fast-ion losses measured with FILD1 and FILD2 and timing of MP coil currents.

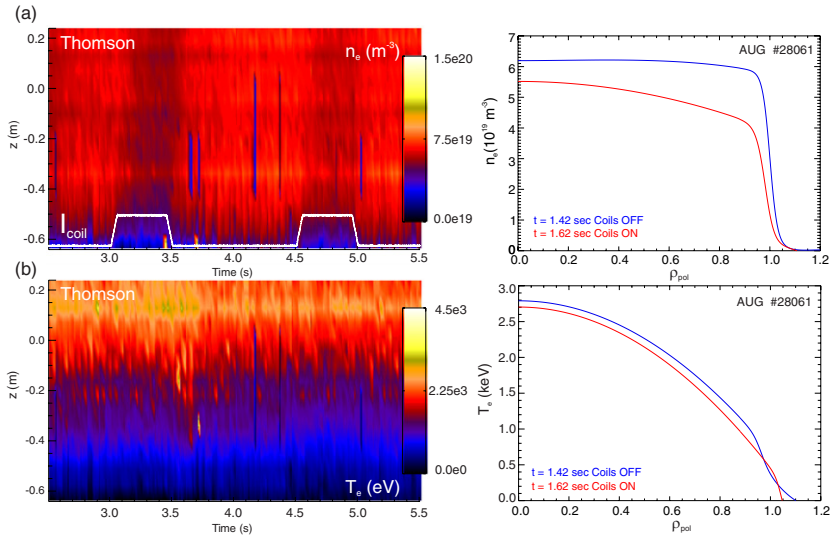

Figure 5. AUG discharge #28061. Temporal evolution of T_e and n_e profiles measured by TS with and without MPs.

by the external perturbation. The effect of the density pump-out is also clearly visible in the beam emission spectroscopy (BES) signal as shown in figure 6. The lower density during the MP phase leads to a deeper beam deposition and an apparent (large change in n_e but not in T_e) displacement of the separatrix of ≈2–3 cm. MHD spectroscopy plays an important role when studying the plasma response to externally applied MPs and estimating the field penetration. In the present discharge a (3, 2) NTM gets partially stabilized when applying the external MPs as it slows down in the background plasma. Figure 7(*a*) shows the spectrogram of a magnetic pick-up coil with the coils timing highlighted in white. A tangential beam (NBI#7), responsible for the higher nominal NTM frequency until $t = 4.0$ s, is replaced with a radial beam (NBI#5) with the corresponding drop in plasma rotation, visible in CXRS and the NTM frequency. The (3, 2) NTM frequency drops up to 30% when the MP coils are switched on (with an apparent saturation frequency) achieving again rapidly its original nominal frequency when the MP coils are switched off. An estimation of the electromagnetic torque imposed by the coils' fields on the (3, 2) magnetic island that seems to lead to this island braking will be the subject of a dedicated publication [32].

In KSTAR, a strong plasma response, i.e. density pump-out and plasma braking, to resonant $n = 1$ and $n = 2$ MPs is typically observed in discharges with low q_{95} and intermediate to low collisionality whereas little to no effect is observed with non-resonant MP coil configurations.

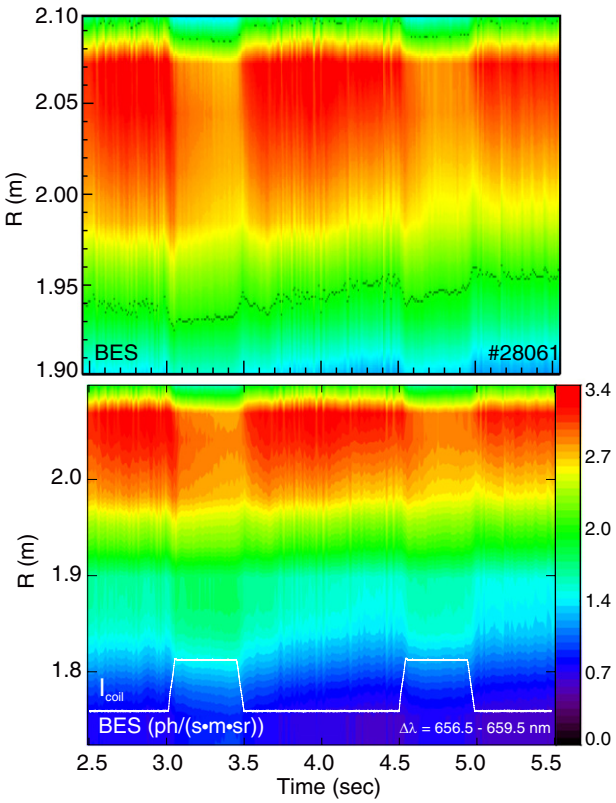

Figure 6. AUG discharge #28061. Temporal evolution of the beam emission profile measured with the AUG BES diagnostic. (*a*) is a zoom in the radial coordinate of (*b*).

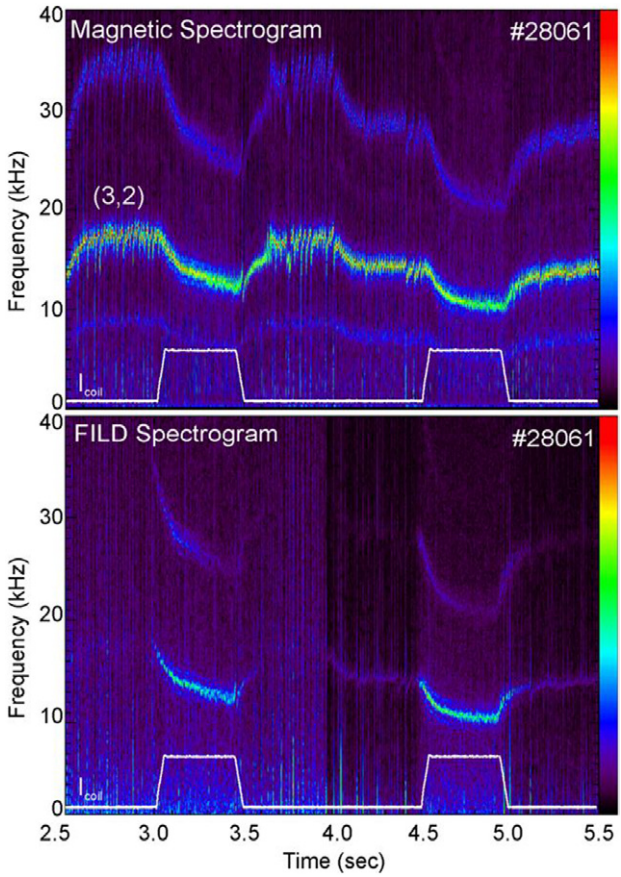

Figure 7. AUG discharge #28061. Spectrogram of (*a*) magnetic pick-up coil and (*b*) fast-ion losses measured by FILD1.

3.2. Fast-ion dynamics in the presence of MPs

In low-collisionality AUG and KSTAR plasmas the application of externally applied MPs is often accompanied by a rather large loss of fast-ions with a broad-band frequency and amplitude correlated with the current of the MP coils. FILD measures at different locations an additional loss of fast-ions during the MP phase that can be up to an order of magnitude higher than the NBI prompt loss signal without MPs. The fast-ion response to MPs is, however, a complex 3D problem rather sensitive to the MP field penetration and overall plasma response. In the AUG discharge presented here, two FILD detectors were operating simultaneously with impressive differences in their signals. Figure 4 shows the temporal evolution of the downsampled FILD1 and FILD2 signals. While FILD1 signals clearly rise when the coils are on, the FILD2 signals drop dramatically. The time traces of two different pitch-angles and the same energy ($E \approx 80$ keV) show some important differences in FILD1, with FILD2 signals having the same temporal evolution for both pitch-angles.

The velocity-space of the escaping NBI ions measured by FILD identifies unequivocally the orbit topology of the ions that are most affected by the perturbation fields while multiple local FILD measurements helps understanding the 3D effect, in real space, of the MPs on the fast-ion distribution function. In figure 8, the energy and pitch-angle of the escaping ions measured by FILD1 with and without the MP coils during the different NBI phases are shown. Figures 8(*a*), coils OFF, and (*b*), coils ON, correspond to the NBI#3+#8 phase. Figures 8(*c*), coils OFF, and (*d*), coils ON, correspond to the NBI#3+#7 phase and figures 8(*e*), coils OFF, and (*f*), coils ON to the NBI#3+#5 phase. Figures 8(*a*), (*c*) and (*e*) give an overview of the NBI prompt losses, with ≈93 keV, measured by FILD1 while figures 8(*b*), (*d*) and (*f*) show the new velocity-space areas covered with fast-ion losses due to the MP coils. In all cases, fast-ion losses with gyroradii ≈30–40 mm and pitch-angles ≈60° appear only when the MP coils are ON. Figures 8(*b*) and (*d*) show, in addition, other energies and pitch-angles that without the MPs would be well confined. A Fourier analysis of the fast-ion loss signal, figure 7(*b*), reveals that the (3, 2) NTM is not causing any significant fast-ion loss until the MP coils are switched on, indicating a possible coupling between the internal (3, 2) NTM transport and the effect of the external $n = 2$ MP.

In AUG, the temporal evolution of the confined fast-ion profiles has been monitored with tangential and vertical active FIDA diagnostics. As the spectra covered by the tangential FIDA diagnostic includes the beam emission, one can infer a direct measure of the fast-ion content accounting for changes in beam deposition due to density pump-out. Figure 9 shows the temporal evolution of the FIDA emission (*a*), beam emission (same as in figure 6 but with less edge channels), (*b*), and fast-ion content, (*c*), profiles. A clear enhancement of the FIDA emission is visible when the MP coils are ON in both NBI phases. In fact, this enhancement of the FIDA emission is due to larger content of confined fast-ions during the MP phase and not only due to a deeper deposition of NBI neutrals, as figure 9(*c*) shows with FIDA/BES. The lower collisionality

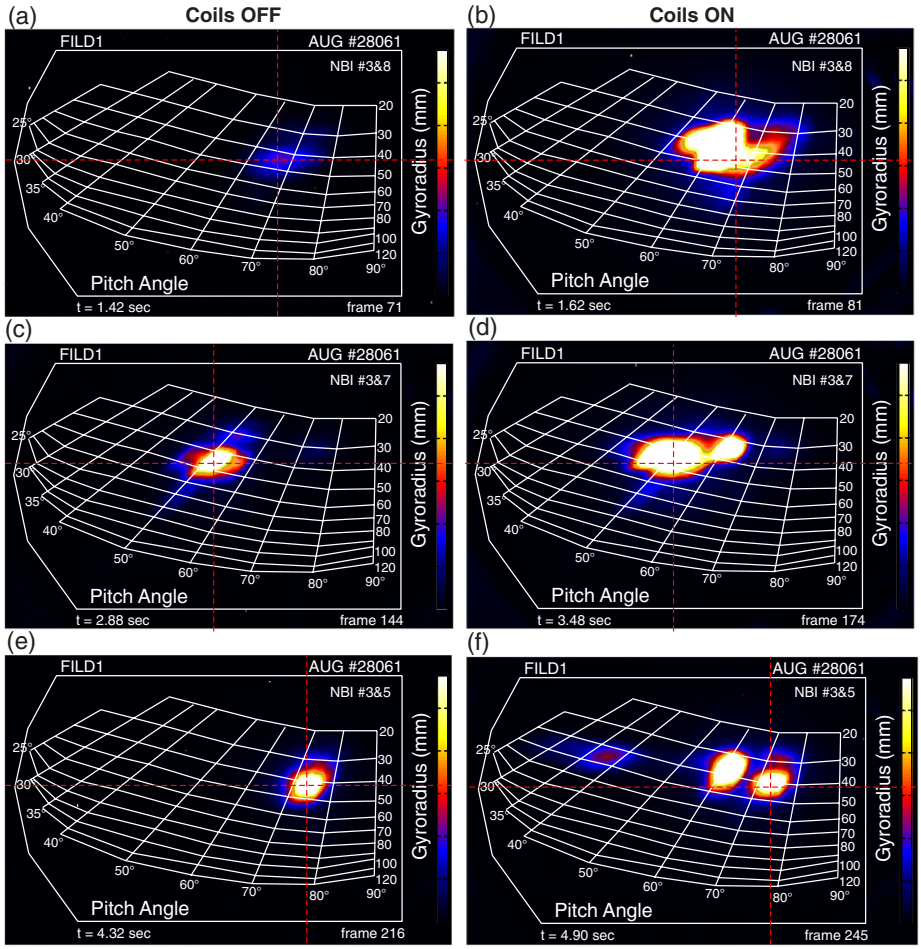

Figure 8. AUG discharge #28061. Velocity-space of escaping ions measured by FILD1 with MP coils OFF, (*a*), (*c*) and (*e*) and with MP coils ON, (*b*), (*d*) and (*f*).

due to density pump-out could account for the larger fast-ion content observed during the MP phases.

Previous simulations of fast-ion losses induced by externally applied MPs have shown a reasonable agreement between measurements and simulations in AUG plasmas with high collisionality and weak fast-ion response [33]. The strong impact that collisionality has on the thermal and suprathermal plasma response and ultimately on the final fast-ion wall loads remains to be understood.

Experiments at KSTAR have been executed to investigate the effect of external MPs on the fast-ion content with different MP toroidal mode numbers and resonant/non-resonant configurations. As in AUG experiments, the overall fast-ion response closely follows that of the main plasma, e.g. electron density. A large density pump-out and plasma braking is typically observed at KSTAR with resonant MP configurations which is normally accompanied by high fluxes of fast-ion losses measured by FILD. In contrast to this, external MPs with non-resonant configurations have little to no effect on the main plasma parameters and fast-ion transport. Figures 10(*a*) and (*b*) show the temporal evolution of the line-integrated density and current of MP coils for two shots with a resonant (#7390) and a non-resonant (#7453) $n = 1$ MP coil configuration. The fast-ion losses measured in the discharge with a resonant MP coil configuration is shown in figure 10(*c*). In the resonant case (#7390), a density pump-out of up to $\approx$50% during the maximum MP coil current is accompanied by a rapid increase in the fast-ion losses. In the non-resonant case, however, no response to the external MPs is observed even with a coil current of up to 8 kA (note that with a resonant configuration MP coils cannot be run at their maximum current at KSTAR to avoid plasma disruptions). The velocity-space of the measured escaping ions during the resonant MP phase is shown in figure 11(*b*) while figure 11(*a*) shows, in contrast, the typical NBI prompt losses measured in the same discharge without externally applied MPs. The MP effect is visible not only in the brighter intensity of the signal, i.e. stronger losses, but also in the velocity-space of the escaping ions covering a broader pitch-angle and energy range. In general, the overall fast-ion response to externally applied MPs closely follows the response of the main plasma.

4. Conclusions

A strong interaction between fast-ions and spontaneous and externally applied edge perturbations have been observed in the AUG, DIII-D and KSTAR tokamaks. Two phases can be clearly distinguished in ELM-induced fast-ion losses with respect to the ELM cycle; inter- and intra-ELM losses. A pre-ELM coherent modulation of the edge density is often

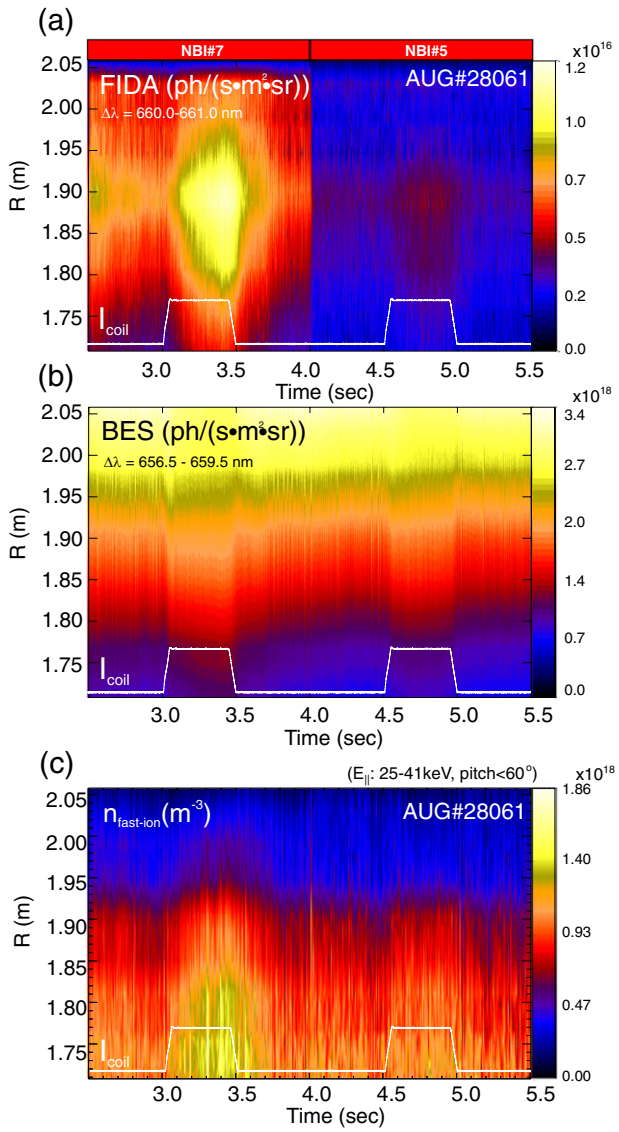

Figure 9. AUG discharge #28061. FIDA diagnostic. (*a*) FIDA emission, (*b*) beam emission (BES) and (*c*) fast-ion content (FIDA/BES).

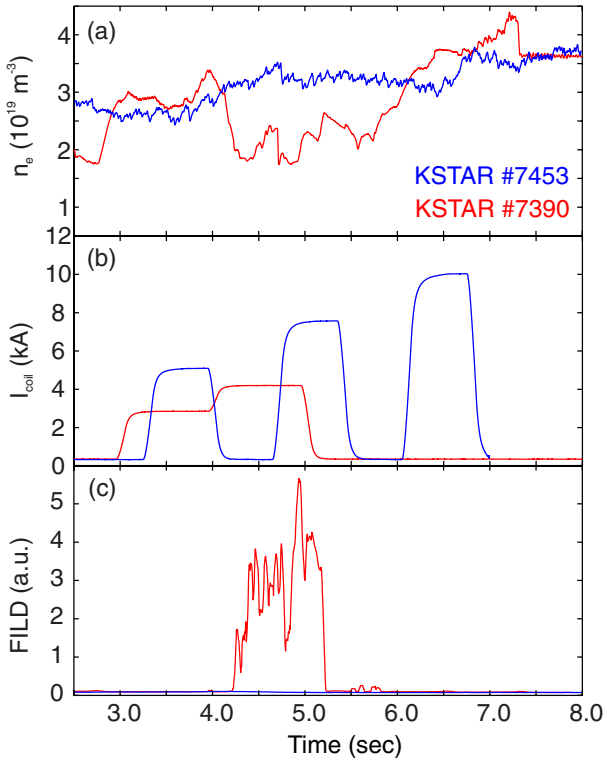

Figure 10. KSTAR. Plasma response to resonant (#7390) and non-resonant (#7453) MP configurations. Temporal evolution of (*a*) line-integrated density, (*b*) $n = 1$ MP coil current and (*c*) fast-ion losses.

correlated with the observed fast-ion losses. The amplitude of the fast-ion losses increases towards the ELM crash while the amplitude of the density perturbation does not. Intra-ELM losses feature often a filament-like fashion with several well-defined bursts within an ELM.

In low-collisionality H-mode plasmas, externally applied MPs have a dramatic impact on fast-ion dynamics. A clear enhancement of the fast-ion content is measured by FIDA during MP phases, following the temporal evolution of the density pump-out. MP-induced fast-ion losses may be up to an order of magnitude higher than the NBI prompt loss signal without MPs as measured by several FILD systems located at different toroidal and poloidal positions. The results presented here indicate that the synergistic effect of externally applied MPs and internal fluctuations should be taken into account when calculating the additional transport induced by external MPs. Indeed, if the MP fields are not efficiently screened by the plasma, the loss boundary may be moved inwards by additional transport mechanisms, e.g. stochasticity, populating the loss cone with ions that would, otherwise, be well confined. This could be of special significance if the loss boundary is pushed to the vicinity of internal fluctuations, e.g. magnetic islands, in particle phase-space. In fact, measured fast-ion losses show a broad energy and pitch-angle range and are typically on banana orbits that explore the entire pedestal/scrape-off-layer (SOL) that could easily interact with internal and external perturbations on their banana orbit. Simulations of the experimental results presented here will be performed using MP fields calculated in vacuum, as already carried out for AUG [33] and ITER [34], as well as with different plasma shielding models. In view of ITER, the detailed fast-ion measurements presented here will contribute to a better understanding of the interaction between fast-ions and MP fields and will likely constitute an important step towards the validation of plasma response and fast-ion transport codes. Special care of the possible impact that the MP-modified fast-ion profiles, in particular off-axis NBI profiles, may have in ITER MHD stability (including Alfvén eigenmodes) and first-wall localized heat load should be taken. The inclusion of fast-ions in future edge stability codes may help to explain why the ELM frequency increases or why ELMs are suppressed when MPs are applied specially in ITER-relevant low-collisionality plasmas.

Acknowledgments

This research was supported in part by the Spanish Ministry of Economy and Competitiveness (RYC-2011-09152

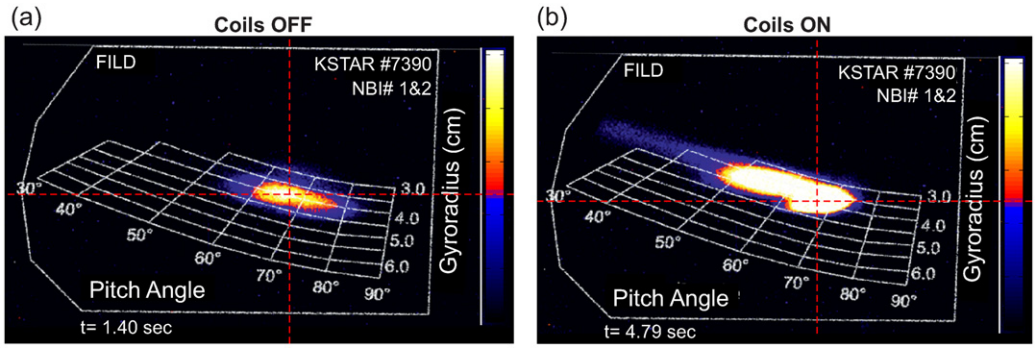

Figure 11. KSTAR discharge #7390. Fast-ion losses measured by KSTAR FILD during MPs.

and ENE2012-31087), a Marie Curie FP7 Integration Grant (PCIG11-GA-2012-321455), the US Department of Energy under DE-FC02-04ER54698, SC-G903402, DE-FG02-04ER54761, DE-AC02-09CH11466 and DE-FG02-08ER54984, the NRF Korea contract 2009-0082012 and the MEST under the KSTAR project.

References

[1] Wagner F. *et al* 1982 *Phys. Rev. Lett.* **49** 1408
[2] Wagner F. *et al* 1984 *Phys. Rev. Lett.* **53** 1453
[3] Zohm H. 1996 *Plasma Phys. Control. Fusion* **38** 105
[4] Federici G. *et al* 2003 *Plasma Phys. Control. Fusion* **45** 1523
[5] Loarte A. *et al* 2003 *Plasma Phys. Control. Fusion* **45** 1549
[6] Pitts R.A. 2011 *J. Nucl. Mater.* **363** 1093
[7] Snyder P. *et al* 2004 *Nucl. Fusion* **44** 320
[8] Hender T. *et al* 1992 *Nucl. Fusion* **32** 2091
[9] Liang Y. *et al* 2007 *Phys. Rev. Lett.* **98** 265004
[10] Evans T.E. *et al* 2004 *Phys. Rev. Lett.* **92** 235003
[11] Suttrop W. *et al* 2011 *Phys. Rev. Lett.* **106** 225004
[12] Okabayashi M. *et al* 2005 *Nucl. Fusion* **45** 1715
[13] Hu Q. *et al* 2012 *Nucl. Fusion* **52** 083011
[14] Haye R.J.L. *et al* 2002 *Phys. Plasmas* **9** 2051
[15] Rechester A.B. and Rosenbluth M.N. 1978 *Phys. Rev. Lett.* **40** 38
[16] Heikinnen J.A. and Lonnroth J. 2007 *Plasma Phys. Control. Fusion* **49** B465
[17] Turnbull A. 2012 *Nucl. Fusion* **52** 054016
[18] Matsunaga G. *et al* 2010 *Nucl. Fusion* **50** 084003
[19] Garcia-Munoz M. *et al* 2009 *Rev. Sci. Instrum.* **80** 053503
[20] Fisher R.K. *et al* 2010 *Rev. Sci. Instrum.* **81** 10D307
[21] Kim J. *et al* 2012 *Rev. Sci. Instrum.* **83** 10D305
[22] Heidbrink W.W. *et al* 2004 *Plasma Phys. Control. Fusion* **46** 1855
[23] Geiger B. *et al* 2011 *Plasma Phys. Control. Fusion* **53** 065010
[24] Rathgeber S.K. *et al* 2013 *Plasma Phys. Control. Fusion* **55** 025004
[25] Classen I. *et al* 2010 *Rev. Sci. Instrum.* **81** 10D929
[26] Igochine V. *et al* 2010 *IPP Report* No 1/338
[27] Silva A. *et al* 1999 *Rev. Sci. Instrum.* **70** 1072
[28] Willensdorfer M. *et al* 2012 *Rev. Sci. Instrum.* **83** 023501
[29] Helander P. 2005 *Phys. Plasmas* **12** 112503
[30] Clements K.G. and Thyagaraja A. 2006 *Phys. Plasmas* **13** 042503
[31] Viezzer E. *et al* 2012 *Rev. Sci. Instrum.* **83** 103501
[32] Fietz S. *et al* in preparation
[33] Asunta O. *et al* 2012 *Nucl. Fusion* **52** 094014
[34] Shinohara K. *et al* 2012 *Nucl. Fusion* **52** 094008